

# Control Performance Analysis of Load-Based Testing for Air-Conditioning and Heat Pump Systems: Part II - Control Analysis, Design, and Validation

Chibuoke Eneh, Jie Ma, James E. Braun, W. Travis Horton, and  
Jie Cai\*

*Ray W. Herrick Laboratories, Purdue University, West Lafayette, IN,  
47906, USA*

---

## Abstract

Air-conditioning and heat pump (ACHP) systems are traditionally rated using steady-state performance tests conducted under fixed indoor and outdoor conditions, with pre-defined compressor and fan speeds. However, an ACHP system's field performance can differ significantly from such steady-state laboratory ratings because of the building load dynamics and their interactions with the native controller. To address this limitation, a load-based testing methodology has been developed to evaluate the dynamic performance of an ACHP system operated under its native controller. This approach emulates a typical building's load and thermal dynamics in a controlled laboratory setting, allowing the unit to respond naturally to changing indoor and outdoor conditions as it would in the field. Therefore, it is expected to

---

\*Corresponding author ([cai40@purdue.edu](mailto:cai40@purdue.edu)).

better characterize an ACHP’s field performance. This new dynamic testing methodology has been adopted by various standards such as CSA SPE-07 and AHRI 210/240. Numerous studies have evaluated the testing procedures in the laboratory, and almost all units tested exhibited oscillatory or cycling behaviors that should not occur for variable-speed systems. These erratic behaviors can degrade an ACHP’s field performance and lead to issues in performance ratings such as failures to earn variable-speed certification, long testing times, and poor reproducibility. This paper presents a control stability and performance analysis framework using a linearized simulation toolkit developed in a companion paper [1]. Control performance impacts of the thermostat and testing facility dynamics and the adopted virtual building model are presented. Informed by the control analyses, a proportional-integral and lead controller was proposed to accelerate the closed-loop response, while ensuring an adequate stability margin. Performance of the proposed controller was demonstrated through both simulation and experimental tests subject to different load-based testing configurations and virtual load models. The proposed controller was shown to achieve almost perfect load and temperature tracking performances with much reduced testing time.

*Keywords:* Load-Based Testing, Air Conditioners and Heat Pumps, Performance Rating Standard, Feedback Control Analysis

---

## 1. INTRODUCTION

In the United States, residential air conditioners and heat pumps (ACHPs) are rated under the Air-Conditioning, Heating, and Refrigeration Institute (AHRI) Standard 210/240-2023 [2], which uses steady-state performance

measurements at specified indoor and outdoor conditions in conjunction with a temperature-bin approach to calculate seasonal efficiency metrics such as the Seasonal Energy Efficiency Ratio (SEER) and the Heating Seasonal Performance Factor (HSPF). While this enables performance comparisons across manufacturers, it doesn't include testing with the unit's integrated controls and ignores the interactions with the actual building environment. Early studies observed discrepancies up to 35% in SEER values between regulatory steady-state tests conducted in testing facilities and real-world operation of heat pump units [3, 4].

To address these gaps, the industry and regulatory agencies are developing dynamic, load-based testing methods that characterize an ACHP system's performance under native control with simulated dynamics for the indoor environment. This dynamic performance testing approach has been adopted by the CSA SPE-07:23 [5] and has been added to AHRI 210/240-2023 [2] as Appendix I, which describes a Control Verification Procedure (CVP) following a load-based testing method. Several studies have demonstrated the feasibility and superiority of load-based testing methods over traditional steady-state rating approaches. Cremaschi and Paez conducted a laboratory feasibility study of load-based testing for a light commercial AC system [6]. Hjortland et al. [7] applied it for performance assessments of constant- and variable-speed rooftop units, finding significant deviations from steady-state performance under part-load conditions and underscoring the need for climate- and building-specific metrics. Patil et al. [8] compared performance ratings for a 5-ton heat pump and found steady-state methods overestimated seasonal performance by 22–27%. Building on this, Cheng

et al. [9] developed convergence criteria and standardized procedures with improved consistency and reproducibility. Dhillon et al. [10, 11, 12, 13] have consistently demonstrated that load-based testing could more accurately capture an ACHP system’s performance, providing detailed analyses of seasonal discrepancies and recommendations to improve load-based testing procedures.

Load-based testing has its roots in a more general testing methodology that has existed for a long time - hardware-in-the-loop (HIL) testing. A HIL test integrates both software and hardware components in a single test to evaluate component- (mostly hardware) or system-level performance when testing with all hardware components is infeasible. It provides a powerful tool for early-stage controller design and prototyping, and has been adopted by different disciplines and industries [14, 15, 16]. Some of the first applications of HIL testing in buildings are the International Energy Agency (IEA) Annex 17 and European SIMTEST projects that pioneered testing methods for HVAC control systems aided by building emulation, connecting real controllers to virtual building and plant models to facilitate market introduction of advanced control technologies [17, 18]. However, the developed HIL test bed was software-dominant, with the controller being the only hardware component. More recent HIL research in buildings involved more physical components in the HIL tests. A common HIL experimental setup involves a physical ACHP system coupled to an emulator for the dynamics of the building envelope, which has been adopted for investigating an ACHP system’s interactions with buildings and the power grid [19, 20, 21, 22].

The increasing adoption of variable frequency drives in ACHP systems

offers significant energy efficiency potential, but involves more sophisticated control algorithms that would require a dynamic testing approach to best characterize their performance and quantify the benefits over fixed-capacity counterparts. This is a critical step toward incentivizing the adoption and continuous innovation of energy efficient ACHPs. The newly added CVP in AHRI 210/240 is exactly aimed at (1) certifying variable-speed equipment based on whether a variable-speed ACHP system provides an effective capacity modulation at part load and (2) verifying the consistency between the claimed efficiency rating and actual performance under native control. Reid [23] highlighted the importance of improved control strategies of variable-speed AC systems to attaining high SEER ratings. The studies in [24, 25] presented multi-input multi-output (MIMO) control strategies to achieve simultaneous control of indoor temperature and humidity through compressor and indoor blower speed modulation, enabling accurate control of both sensible and latent capacity. Cai and Braun [26] developed a heuristic control strategy for near-optimal coordination of compressor and fan speeds to maximize operational efficiency of direct-expansion cooling systems. The benefits of such advanced control developments for ACHP systems can be best quantified and demonstrated via load-based testing.

In a load-based test, the testing chamber needs to accurately track time-varying temperature and humidity setpoints, generated by a virtual dynamic building model based on the real-time capacity measurements and load estimation. This represents a challenge for existing mechanical and control systems of a testing chamber, which are primarily designed to facilitate steady-state performance testing. Advanced control strategies may need to be im-

plemented to achieve fast and reliable setpoint tracking to accommodate dynamic load-based tests. Although validation studies have demonstrated the feasibility of load-based testing, its successful adoption by next-generation rating standards requires a comprehensive evaluation of the methodology's ability to accurately capture a system's dynamic field performance in laboratory settings. Giannetti et al. [27] investigated a range of factors that influence the reliability and reproducibility of dynamic measurements in psychrometric chambers. Their analysis considered the dynamics of the chamber's reconditioning system and the temperature and humidity sensors, and the thermal and moisture characteristics of the chamber envelope. Collectively, these factors contribute to slow chamber dynamics, which not only pose a significant control challenge for dynamic load-based testing but also affect the reproducibility of results across different testing facilities. To improve dynamic temperature tracking performance, Giannetti et al. [28] developed a feed-forward compensation strategy for emulator-type testing facilities used in dynamic load-based testing. In their approach, linear dynamic models were estimated for the testing chamber and incorporated in a feed-forward loop to determine predictive control actions. The study demonstrated that feed-forward compensation could reduce the delay in the return air temperature tracking to within 60 seconds across different testing conditions, while enhancing reproducibility of load-based tests to limit performance deviations to within 2%.

The two studies by Giannetti et al. addressed the dynamics and control strategies for testing chambers to accommodate load-based testing. However, other component dynamics, such as those for the thermostat, virtual building

model, and heat pump test unit, were not considered, but could influence the closed-loop response of the heat pump and impact the accuracy of load-based testing approaches. For example, in [27], tests were conducted with the thermostat placed in the return air stream of the indoor unit, which could result in much faster responses than what would be seen in the field. To fill the void, a companion paper [1] presents a holistic simulation framework that captures the dynamics and interactions across all key components involved in a load-based test, including the testing chamber, thermostat, test heat pump, and load controllers. The study showed that the thermostat has slower dynamics than the testing chamber and thereby plays a more important role in the closed-loop response and for controller design.

The Purdue team has conducted load-based CVP tests of four ACHP units provided by different manufacturers, and they all exhibited oscillatory or even cyclic behaviors [29, 13, 30]. The unsatisfactory control performance led to a variety of negative impacts, including failures to earn variable-speed certification, lower efficiency ratings, and high test burden. If the cyclic behaviors are also present in the field operation, additional concerns could arise related to operational efficiency, indoor comfort, and equipment lifespan. Understanding the dynamics and control interactions between the different components in load-based testing is a critical step toward identifying the root causes of unsatisfactory control behaviors and developing improved control strategies. Leveraging the simulation and analysis tool developed in the companion paper [1], this study presents a control stability and performance analysis framework for the load-based testing methodology. Based on the control analysis, we propose a PI plus lead controller to accelerate

and stabilize indoor temperature control against dynamic load conditions of a building. Simulation and experimental test results are presented for three scenarios representing cases with different thermostat and chamber responses. The CSA SPE-07 and AHRI 210/240 CVP procedures involve different virtual building models, and their impact on the closed-loop system response is also analyzed through both simulation and experimental tests.

## 2. Background

### 2.1. Overview of Load-Based Testing Methodology

Figure 1 depicts a typical laboratory setup for load-based testing with twin psychrometric chambers reproducing desired indoor and outdoor conditions for performance assessments of ACHP systems. During a load-based test, a virtual building model is used to calculate the virtual indoor air temperature, which is sent to the reconditioning system of the indoor chamber as its setpoint. The outdoor chamber temperature typically follows a pre-determined trajectory. The virtual building model employs a lumped capacitance approach to predict the virtual indoor temperature based on a sensible energy balance:

$$C_s \frac{dT_{ID}}{dt} = \dot{Q}_{BL,s} - \dot{Q}_s \quad (1)$$

where  $T_{ID}$  is the virtual indoor temperature and  $\dot{Q}_s$  is the measured sensible heating (negative) or cooling (positive) rate delivered by the test unit.  $\dot{Q}_{BL,s}$  is the emulated sensible building load that can be calculated by

$$\dot{Q}_{BL,s} = UA(T_{OD} - T_{BAL}) \quad (2)$$

where  $UA$  is the overall thermal conductance of the building envelope,  $T_{OD}$  is the outdoor temperature, and  $T_{BAL}$  is the balance outdoor temperature

(temperature at which the net cooling or heating load becomes zero after accounting for internal gains). Both CVP and CSA adopt the above virtual building model form, but differ in the method used to calculate  $UA$  and  $T_{BAL}$ . In the CSA load model, the balance outdoor temperature  $T_{BAL}$  is dependent on the indoor temperature  $T_{ID}$ , while the CVP load model relates  $T_{BAL}$  to the test unit thermostat setpoint and is constant. This difference causes the transfer functions of two load models to have different forms with different controller design requirements - the CSA model transfer function has a standard first-order form, while the CVP load transfer function is a simple integrator. The details can be found in the companion paper [1].

This study uses CVP tests to highlight control issues observed with current heat pump controllers and the overall testing methodology. The CVP is primarily employed to (1) determine whether an ACHP system should be rated as a variable-speed or staged unit and (2) verify the consistency in the performance between the native control operation and regulatory control override. The cooling CVP consists of three primary load intervals, namely, full, intermediate, and minimum load, connected by two transitional periods that emulate varying outdoor ambient conditions. This sequential approach evaluates system performance across the complete load and outdoor condition ranges under native control. Each load interval begins with specific outdoor dry-bulb temperatures: 95°F for full load, 79-85°F for intermediate load, and 67°F for minimum load. In CVP tests, the test unit thermostat setpoint is fixed at 80°F, and both indoor and outdoor chamber wet-bulb temperature setpoints for the reconditioning systems are fixed.

## *2.2. Example CVP Test Results*

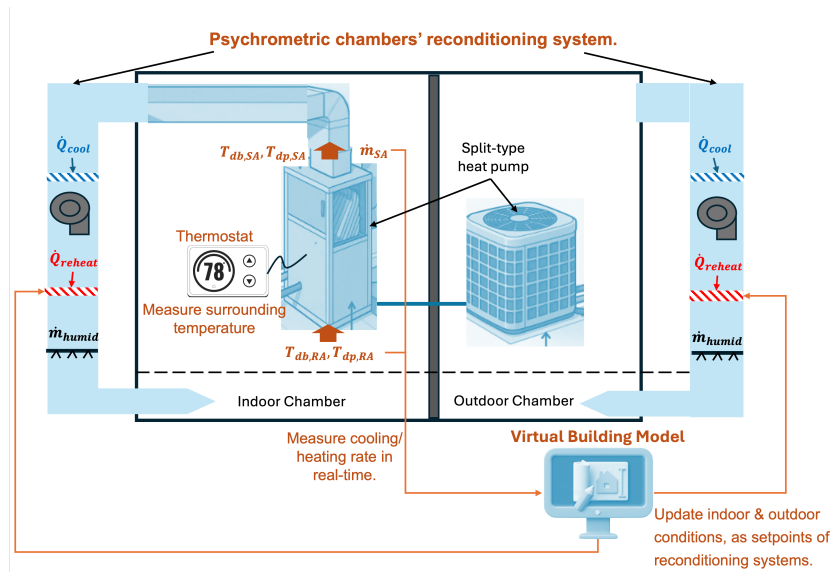


Figure 1: Typical equipment setup for load-based testing. [1]

Figure 2 presents capacity and power variations for a cooling CVP test with a 3-ton variable-speed heat pump. The test was conducted with the thermostat placed on a board within twelve inches from the center point of the return duct vent, per AHRI 210/240 requirement. The test heat pump was able to match the cooling load at the high load interval of the dynamic test, where the compressor and fan speeds saturated at their upper limits, leading to a relatively constant cooling effect. The minor oscillation in the cooling rate was caused by unstable superheat control. The test unit started cycling on and off to meet the load within the first transitional period as the load gradually descended to the intermediate level. In each start-up of a duty cycle, the unit started at the minimum compressor and indoor blower speeds, and then quickly ramped up to the maximum capacity with a trend line characteristic of a PI controller. This led to overcooling of the indoor

space, which eventually triggered the unit to shut down. The cyclic operation continued throughout the rest of the test.

Figure 3 shows the dynamics of the thermostat temperature alongside the return air temperature (RAT, assumed to be a proxy of the indoor chamber temperature) and the virtual indoor temperature generated by the virtual load model. The manufacturer-provided thermostat has a 1°F resolution, resulting in integer-only temperature readings extracted from a video recording of the thermostat display post-processed with a custom image-processing algorithm [31]. The test unit cycled off a few minutes after the thermostat temperature reached its setpoint, and cycled back on when the thermostat temperature stayed beyond its setpoint for a certain duration. This phenomenon implies that a deadband logic is used by the native load controller to determine when to cycle on or off the unit. The CVP involves temperature control tolerance requirements for both indoor and outdoor chambers' reconditioning system - the chamber temperatures should stay within  $\pm 1^\circ\text{F}$  of the respective setpoints. The tolerance bands are presented as green shaded areas in Figure 3. It can be seen that the test failed to meet the control tolerance for both the outdoor and indoor chambers. The temperature excursions were mostly caused by the cyclic operations of the test unit - the abrupt changes in the indoor and outdoor coil heat transfer rates during a cycling event posed significant disturbances to the chambers' reconditioning systems.

The authors have tested four variable-speed heat pumps from different manufacturers using the CVP, and all showed cyclic behaviors similar to the results presented above. The native controller, which constantly forces

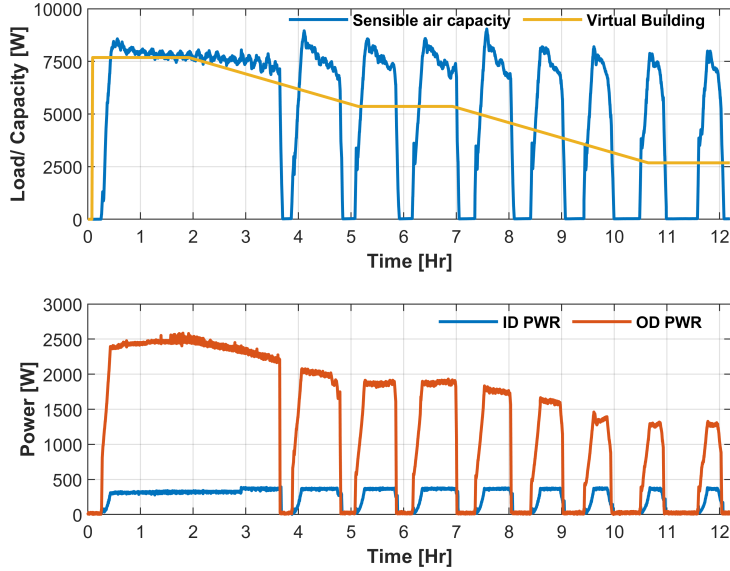


Figure 2: Test unit capacity and power variations for the cooling CVP test under native control.

the test unit into on/off cyclic operations under part-load conditions, causes multiple issues for CVP tests: (1) failure to comply with the chamber temperature control tolerances specified in the standard due to disturbances induced by the cyclic operation of the unit, (2) failure to earn a variable-speed certification (CVP requires that the standard deviation of system power remains within 20% of the mean system power during the intermediate-load interval for the unit to be certified as a variable-speed one), and (3) very high test burden.

### 3. Load-Based Testing Control Analysis Tool

A control simulation and analysis tool was developed in the companion paper [1] that is used for the analysis and development of the heat pump

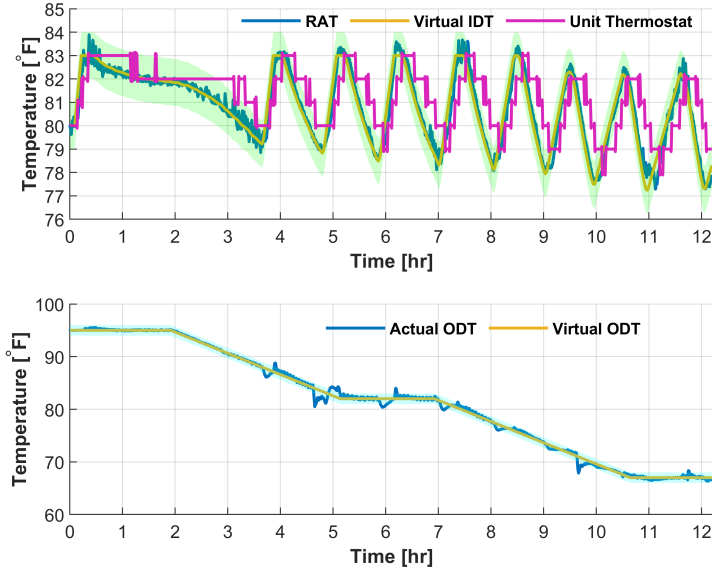


Figure 3: Indoor and outdoor temperature variations for the cooling CVP test under native control.

controller presented in the current study. This section first introduces the common testing infrastructure required for load-based testing and then provides a high-level overview of the component models included in the control analysis tool.

### 3.1. Testing Setup

The load-based testing apparatus is configured within dual psychrometric chambers that provide independent control of indoor and outdoor environmental conditions while enabling real-time interactions between the test unit and virtual building load emulation. A National Instrument CRIO controller is used to monitor the system performance and execute the virtual building model with the measured system capacity and calculated loads in real-time to update the virtual indoor temperature, which is sent to the indoor cham-

ber’s reconditioning system as its setpoint. Baseline control results presented in Figures 2 and 3 were collected with the manufacturer-provided thermostat under its native control. For laboratory tests of the new controller proposed in this study, an emulated thermostat with a model derived from offline thermostat dynamic tests was used in place of the original thermostat, and the determined control commands for the compressor and fan speeds were sent to the heat pump through a proprietary communication protocol provided by the manufacturer. Control of the electronic expansion valve (EXV) was achieved through an external drive board, as the EXV control access is not available through the proprietary communication protocol.

### *3.2. Simulation Model*

A suite of linear dynamic models was developed for all major components involved in a load-based test to facilitate control analysis. Transfer functions of the component models and the respective inputs and outputs are summarized in Table 1. Case III of Figure 4 illustrates a complete feedback control loop involved in a heat pump load-based test. Details of the developed models covering all control blocks therein can be found in [1], while a high-level overview is presented in this section so that the control analysis presented in later sections can be easily followed.

Heat Pump: A heat pump model receives the percentage compressor and supply fan speed as input (%) and outputs sensible cooling capacity (W). This study assumes fully synchronized compressor and fan control with the same percentage speed settings for the two components.

Virtual Building Model: The virtual building model, downstream of the heat pump in the control loop, accepts sensible cooling rate delivered by the heat

Model	Transfer Function	Input	Output
Heat Pump	$G_{hp} = \frac{84.24}{20s+1}$	Compressor & blower speed (%)	Sensible cooling capacity (W)
Virtual Building	CVP: $G_{vb} = \frac{1}{1.187 \times 10^6 s}$ CSA: $G_{vb} = \frac{1}{1.187 \times 10^6 s + 282.5}$	Sensible cooling capacity (W)	Virtual IDT (°F)
Testing Chamber	$G_{chb} = \frac{28.5s+0.047}{3755s^2+29.5s+0.047}$	Virtual IDT (°F)	Zone air temp. (°F)
Thermostat	$G_{stat} = \frac{1}{1200s+1}$	Zone air temp. (°F)	Thermostat temp. (°F)

Table 1: Component models in the load-based testing simulation tool.

pump as its input in  $W$ , and outputs virtual indoor air temperature (°F). The virtual building model is the only component in the control loop without a corresponding physical element in the laboratory setup. Both the CVP and CSA load models are presented in Table 1.

Psychrometric Chamber: The indoor psychrometric chamber model receives the indoor chamber temperature setpoint as its input, and outputs the actual zone temperature (both in °F). This chamber model combines a PI controller for temperature regulation and a first-order energy balance model for the chamber temperature emulation. The chamber’s reconditioning system employs two pairs of cooling coils that provide continuous cooling with a near-constant capacity, while a solid-state relay-controlled electric heater is modulated to raise the supply air temperature for fast and accurate chamber temperature regulation.

Thermostat: The thermostat model accepts the indoor chamber temperature as its input and outputs the measured temperature (°F) used for heat pump load control. It functions as a first-order low-pass filter that characterizes the dynamics of the temperature-sensing element within a thermostat using a lumped capacitance model. The time constant of the thermostat model

was derived from laboratory test results of five thermostats from different manufacturers.

Load Controller: The temperature difference between the thermostat temperature reading and its setpoint is fed to the load controller, which determines the speed commands for the heat pump (%). A baseline PI controller and a proposed PI plus lead controller are considered in this study, to be detailed in the sections to follow.

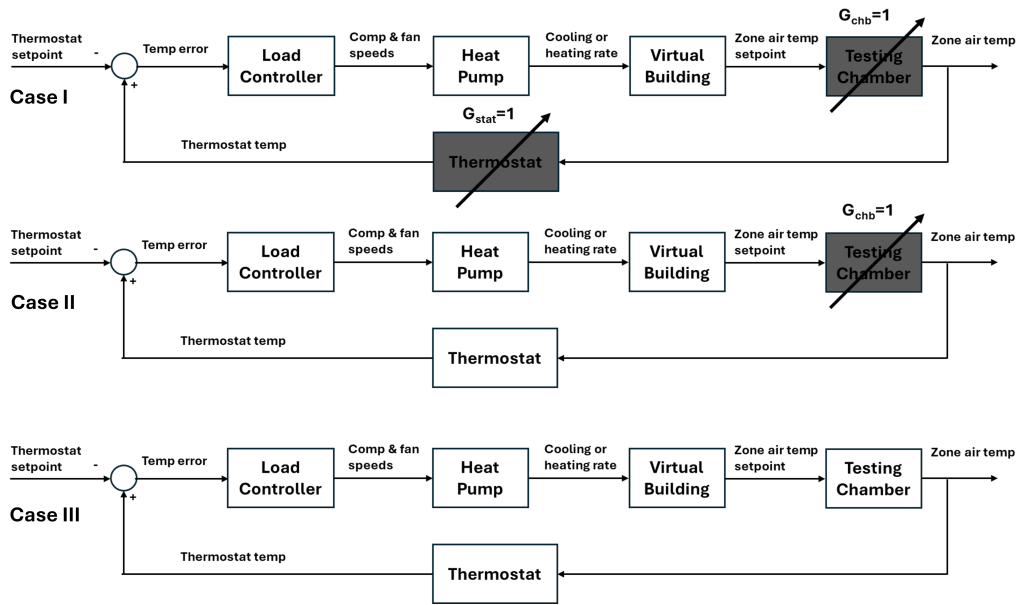


Figure 4: Control diagrams for the three scenarios.

#### 4. Control Performance Analysis

Control analysis is presented for three different scenarios:

- Testing chamber and thermostat dynamics are ignored (Case I - NoChamberNoThermostat);

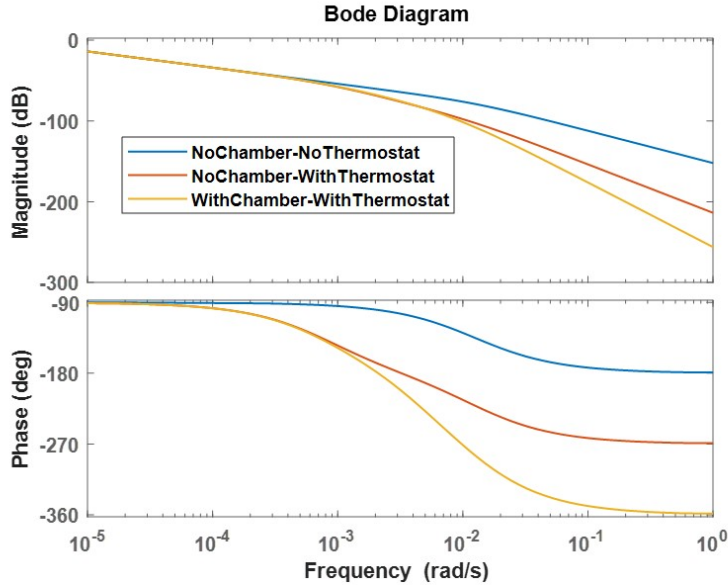


Figure 5: Loop transfer function Bode diagram comparison.

- Testing chamber dynamics are ignored while thermostat dynamics are considered (Case II - NoChamberWithThermostat);
- All dynamics are considered (Case III - WithChamberWithThermostat).

Figure 4 shows control diagrams for the three cases. Case I represents a field operation scenario with a fast-responding thermostat, where chamber dynamics are not involved in the control loop. Typically, thermostats used in commercial buildings have faster responses than those used in residential buildings [32]. Ventilated thermostats, either with an active or passive design, tend to respond faster than those with tight enclosures. Representing an extreme case with the fastest response, Case I provides a benchmark to evaluate the impact of thermostat and testing chamber dynamics on the con-

trollability of the system. Case II is the best representative of a heat pump’s field operation, considering typical residential thermostat dynamics. However, it is difficult to implement or realize in a psychrometric chamber testing environment. Case III represents the most common setting for load-based testing inside psychrometric chambers. However, the test results obtained under this setup are likely to misrepresent a heat pump’s field performance due to the involvement of chamber dynamics which would not be present in a field operation. Using a fast-responding environmental chamber for the thermostat, e.g., the Thermostat Environment Emulator (TEE) proposed in [33], can help reduce the discrepancy when a physical thermostat has to be tested alongside the heat pump. If emulated thermostats are allowed, this issue can be overcome by feeding the virtual indoor temperature, instead of the actual chamber temperature, to the thermostat emulator. This will be re-visited in Sections 5 and 7.

Figure 5 compares Bode diagrams of the following open-loop transfer functions corresponding to the three cases, with a unity-gain load controller  $C = 1$ :

$$\text{Case I: } L_I = C \cdot G_{\text{hp}} \cdot G_{\text{vb}}$$

$$\text{Case II: } L_{II} = C \cdot G_{\text{hp}} \cdot G_{\text{vb}} \cdot G_{\text{stat}}$$

$$\text{Case III: } L_{III} = C \cdot G_{\text{hp}} \cdot G_{\text{vb}} \cdot G_{\text{stat}} \cdot G_{\text{chb}}$$

We are mainly interested in two performance metrics: (1) gain cross-over frequency  $\omega$  and (2) phase margin  $\phi$ . The gain crossover frequency is directly related to the closed-loop response rate, while the stability margin relates to closed-loop stability, overshoot, and severity of oscillation in the closed-loop

response. For a heat pump load controller, a gain crossover frequency above 0.005 rad/s was found to achieve reasonably fast responses from preliminary simulation tests conducted using the control analysis tool. From Figure 5, it is clear that high feedback gains are needed to shift the magnitude curve upward to speed up the response, for all three scenarios. Case I has the fastest response, while Case III, which considers both chamber and thermostat dynamics, has the slowest closed-loop response and thereby requires the highest feedback gain. The phase margin should preferably be kept above  $45^\circ$ , a commonly adopted margin used in feedback controller design to account for model inaccuracies, uncounted disturbances, etc. It is evident from Figure 5 that the slow chamber and thermostat dynamics can sag the phase curves, making it a challenge to meet the phase margin requirement. For Case III, a phase addition of at least  $60^\circ$  is needed to achieve a positive phase margin at  $\omega = 0.005$  rad/s. Achieving a faster response for this case would require a more aggressive phase boost, which may require multiple cascaded lead controllers. These results highlight the control challenges induced by the slow responses of the thermostat and testing chamber.

## 5. Controller Design

A baseline PI controller and its control issues are presented first through simulation tests. To address the identified issues, the PI controller is augmented with a lead control block that adds phase and increases the gain crossover frequency. Simulation test results are presented in this section and Section 6, while experimental validation results and analysis are presented in Section 7.

### 5.1. Simulation Test Design

A simulation test is designed for evaluating the performance of the baseline and proposed controllers. The test sequence consists of the following segments:

- A 25000-second warmup period for the system to reach steady state;
- CVP test sequence with three load intervals and two transitional periods lasting for 30000 s;
- A temperature setpoint change from 73°F to 75°F imposed at 55000 s;
- A change of load from the low-load setting to the intermediate load level imposed at 65000 s.

This test sequence starts with a complete CVP test to evaluate the control responses under a load-based testing setup. However, the CVP mainly aims to assess (1) the load and temperature setpoint tracking performances of the native controller at the intermediate load level and (2) the heat pump efficiency under native control. It does not fully characterize a heat pump's control performance. An actual building is subject to frequent thermostat setpoint changes (e.g., during transitions between occupied and unoccupied modes) and abrupt load variations (e.g., during engagement of cooking or other power-intensive appliances). The last two segments of the simulation tests are geared toward evaluating the setpoint tracking and load disturbance rejection performances of a controller.

## 5.2. Baseline PI Controller

A baseline PI controller is considered, which is commonly used in thermal system applications. The proportional and integral gains were obtained by matching the native control behaviors of the test unit. The baseline control transfer function was determined as:

$$C_{\text{PI}} = \frac{84.5s + 0.00845}{s}.$$

Figure 6 compares the Bode diagrams of the loop transfer functions for the baseline PI controller as well as the gain margin (GM), gain crossover frequency, and phase margin (PM) across the three cases. The dashed vertical lines highlight the gain cross frequencies and the corresponding phase margins. Figures 7 and 8 compare the simulated closed-loop responses in the time domain for the three cases under the baseline PI control. Case I results shown in Figure 6 have the highest gain crossover frequency and phase margin. This is consistent with the simulation results shown in Figures 7 and 8 as Case I involves the fastest response and minimum overshoot. The PI controller works well for this case, meeting the performance requirements discussed in the proceeding section. For Case II, the phase margin and gain crossover frequency are significantly lower, resulting in very slow and oscillatory responses as evident from Figures 7 and 8. This is mainly caused by the slow thermostat dynamics which are neglected in Case I. The closed-loop response is still stable, but can easily become unstable when the operating conditions change and model mismatch emerges. For Case III, the PI controller results in unstable responses with negative margins, caused by the additional dynamics associated with the testing chamber's reconditioning system.

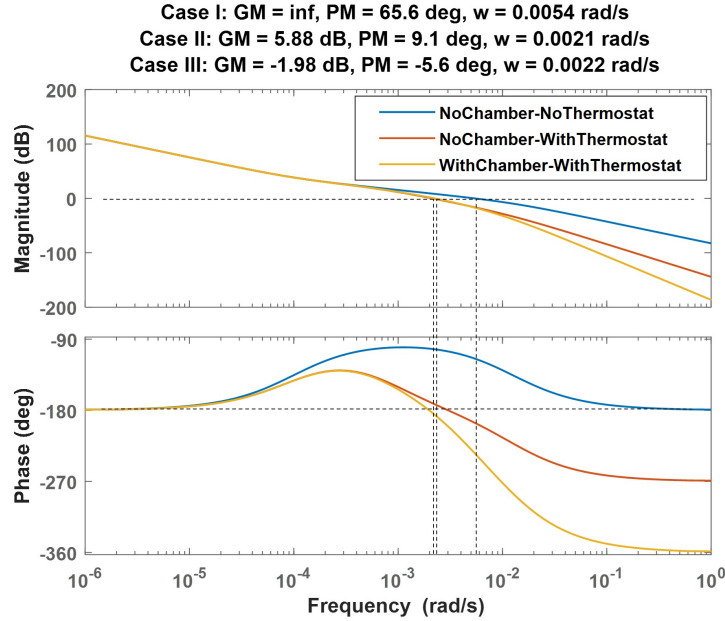


Figure 6: PI control Bode diagram and margins.

Experimental tests were also conducted for the PI controller under Case II and Case III configurations, but only subject to the CVP intermediate load conditions due to the long test durations. The experimental tests led to a consistent outcome - the PI controller can result in stable closed-loop responses for Case II, but becomes unstable for Case III. Detailed experimental results and analysis can be found in [1]. The results clearly highlight the following issues:

- The baseline PI control approach, which is commonly adopted by heat pump controllers, can result in slow and even unstable responses when a slowly responding thermostat is in place. Increasing the control gains could speed up the response, but would reduce the stability margins. A higher-order controller is needed, which is addressed in the following

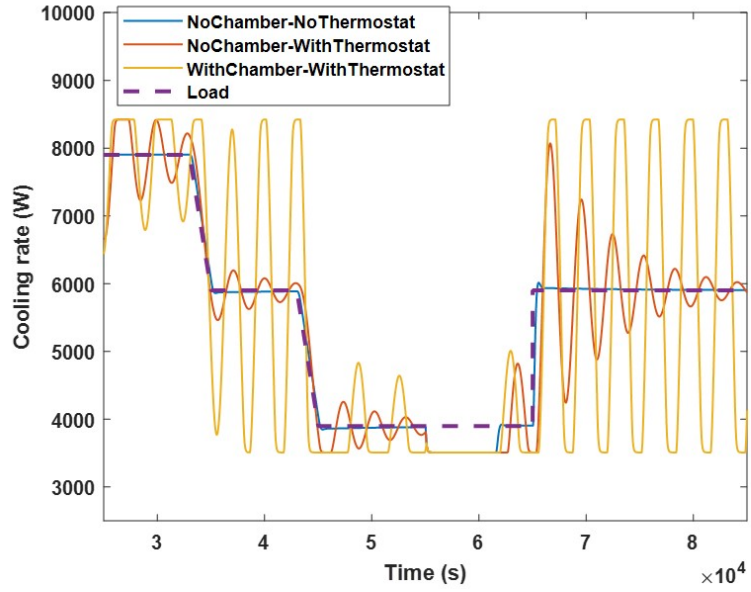


Figure 7: PI control simulation results - cooling rate.

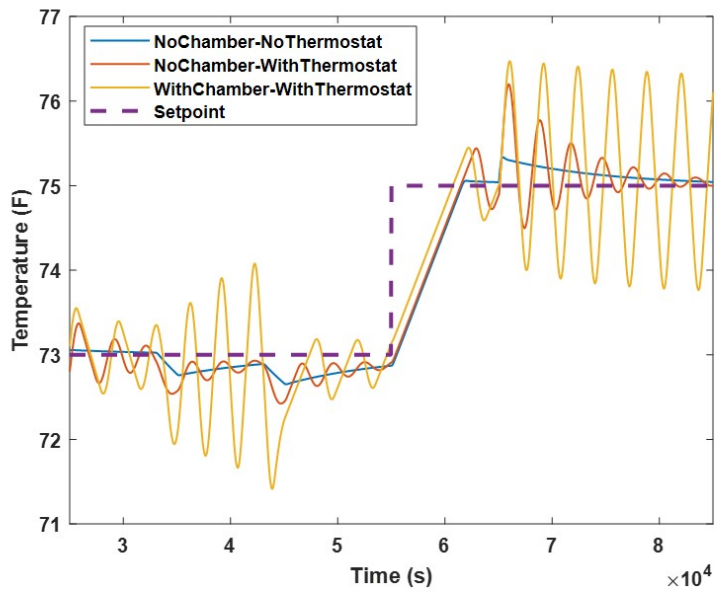


Figure 8: PI control simulation results - temperature.

subsection.

- The load-based testing methodology with the thermostat placed in a psychrometric chamber may mischaracterize a heat pump’s native control performance – the controller can result in unstable response in a testing chamber, which may otherwise be stable in the field. The load-based testing methodology should be modified to address this inconsistency. Recommendations are provided in [1]. It is not a focus of this study.

### 5.3. PI and Lead Controller

The major problem of a PI controller for Cases II and III is that the phase curves sag at high frequencies, leading to low or negative margins, which limits the P gain allowed. Phase addition is needed to overcome this problem and a lead control action is proposed to be used on top of the PI controller - the integral control action is still required to reduce or eliminate steady-state errors. A lead controller has the following transfer function:

$$C_{\text{lead}} = \frac{s/\omega_z + 1}{s/\omega_p + 1}.$$

As shown in Figure 9, a lead controller contributes a peak phase addition of  $\Phi_m$  at frequency  $\omega_m = \sqrt{\omega_p \cdot \omega_z}$ , where  $\Phi_m = \sin^{-1}((\gamma - 1)/(\gamma + 1))$  and  $\gamma = \omega_p/\omega_z$ . A larger value of  $\gamma$  provides more phase addition and adds a gain of  $10 \log \gamma$  at the central frequency  $\omega_m$ . However, an excessively large setting of  $\gamma$  may shift the gain crossover frequency to the right toward the deep phase sagging region. This study used  $\gamma = 100$ , and set the central frequency  $\omega_m = 0.01$  rad/s, higher than the target gain crossover frequency of

0.005 rad/s to compensate for the phase sag for Case III. The final controller, combining the PI and lead actions, has the following transfer function:

$$C = \frac{84.5s + 0.00845}{s} \cdot \frac{1000s + 1}{10s + 1}.$$

This PI+lead controller is designed to provide stable and fast heat pump control under Case II, which best represents a heat pump's field operation. However, the parameter  $\gamma$  is configured to offer a phase boost over a wide frequency spectrum so that reasonable control performance could also be achieved for Case III. Further, this design improves the control robustness against model inaccuracies and unexpected disturbances.

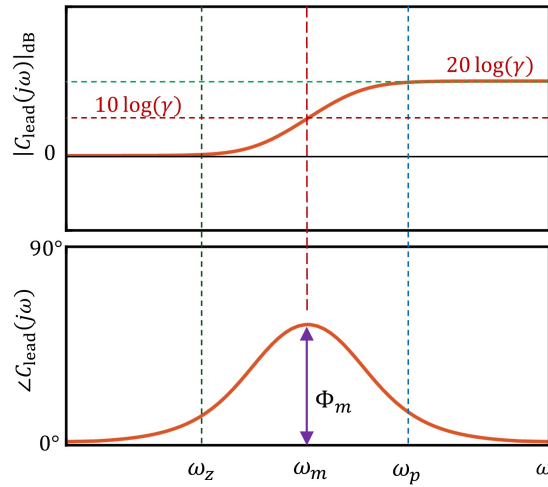


Figure 9: Lead controller Bode diagram.

### 5.3.1. Control Performance Analysis for Case II

Figure 10 compares the Bode diagrams of the unity-feedback, PI, and PI+lead controllers for Case II. It can be seen that the PI controller shifts the magnitude curve to the right, significantly accelerating the closed-loop

response compared to a unity-feedback controller. The PI controller results in a lower phase, but only at low frequencies relative to the unity-feedback controller. The phase margin of the PI controller is very low ( $9.1^\circ$ ), mainly as a result of the gain crossover frequency being shifted to the right. The lead control action more than doubles the gain crossover frequency compared to the PI controller, leading to a further accelerated response (close to the target response rate); more importantly, it boosts the phase margin significantly to  $64^\circ$ .

Figure 11 compares the simulation results of the different controllers for Case II. The top subplot depicts the cooling rate delivered by the heat pump under PI and PI+lead controllers along with the cooling load. The bottom subplot shows the variations of the indoor temperature and its setpoint. The results verify that the PI+lead controller results in a much faster response while completely eliminating oscillations in the settling process.

### *5.3.2. Control Performance Analysis for Case III*

Figure 12 compares the Bode diagrams of the different controllers for Case III. As discussed in Section 5.2, inclusion of the chamber dynamics makes the PI controller unstable with a negative phase margin. The lead control action accelerates the system response while bringing the phase margin to a positive level. However, the phase margin is significantly lower than that of Case II and also lower than the target margin of  $45^\circ$ , caused by the inclusion of the chamber dynamics. Since a phase margin is closely tied to the damping ratio, the reduced margin in Case III results in an oscillatory closed-loop response in the transient periods right after the step changes imposed on the setpoint and load, as evident in Figure 13. However, the overall test performance is

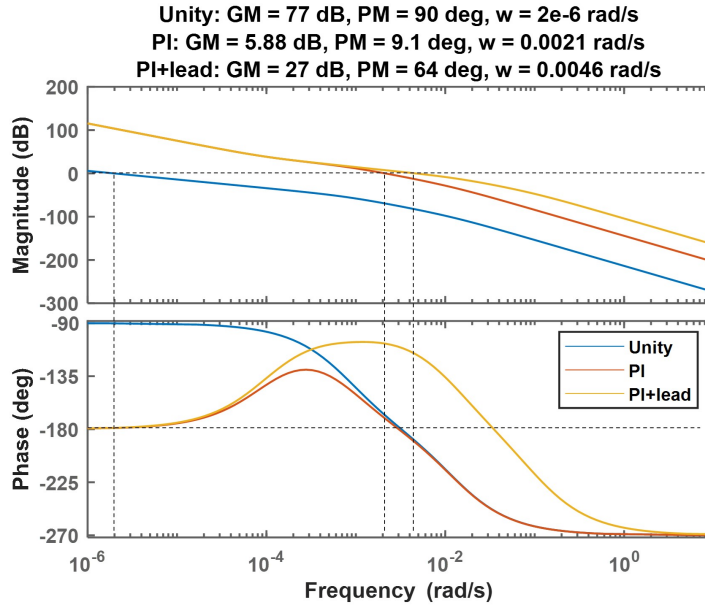


Figure 10: Bode diagram of controllers for case II.

still satisfactory.

The PI+lead controller is shown to provide a fast and stable response, even for Case III with chamber dynamics involved. The controller is also able to provide satisfactory temperature control performance, with maximum errors below  $0.3$  °F, against setpoint adjustments and abrupt load changes. However, some slow residual dynamics can be observed following major load or temperature setpoint changes. This is caused by the “imperfect” cancellation of a pair of closed-loop pole and zero that are very close to each other. This issue can be mitigated by increasing the PI gains (especially the integral gain). It is not pursued in this study since the comfort impact of the residual dynamics is negligible.

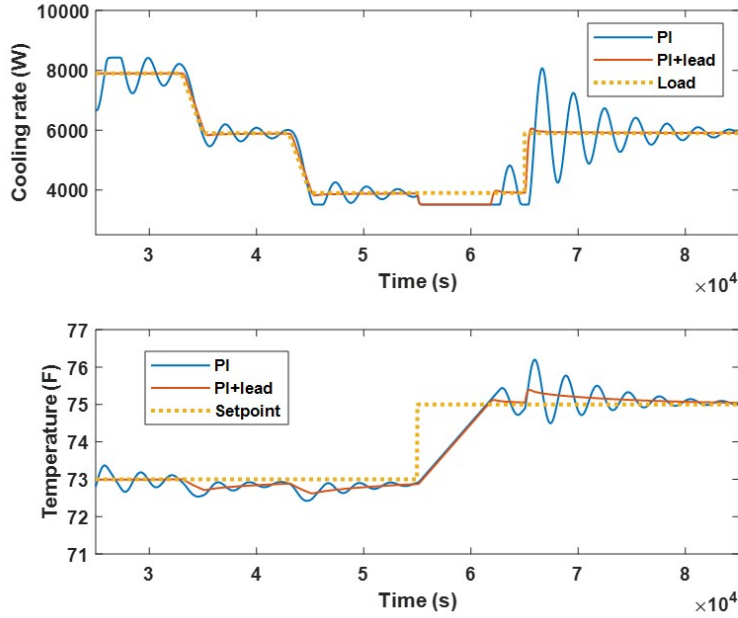


Figure 11: Comparison of controller performances for case II.

## 6. Building Virtual Load Model Impact

The analyses presented above are all based on the CVP load model. However, different building virtual load models can lead to differing closed-loop responses for the same controller. Therefore, it is important to understand the impact of different virtual load models on the control performance. To this end, the above control analyses were repeated for the CSA load model, and the analysis results are compared with the CVP case. Note that the CVP virtual load model is a pure integrator, while the CSA virtual load model has a full first-order transfer function. This leads to different magnitudes and phase angles between the two models only at low frequency ranges, while at intermediate or high frequencies, the two models have similar or identical

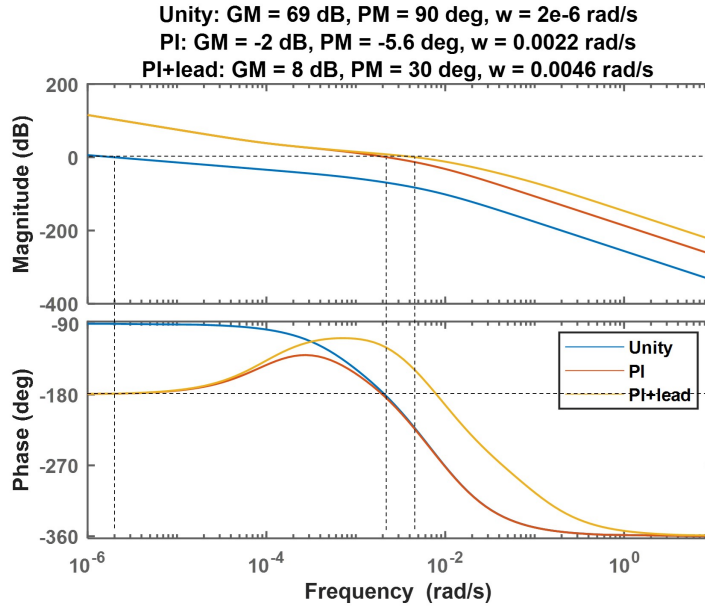


Figure 12: Bode diagram of controllers for case III.

dynamics.

Figure 14 compares the Bode diagrams and phase margins associated with the two load models for the PI controller for Case II. It is clearly seen that the magnitude and phase curves of the two load models overlap at high frequencies but bifurcate when the frequency is reduced. If smaller control gains were used, the CVP load model would result in faster response with the magnitude curve above that of the CSA model. However, the CVP load model involves a constant phase angle of  $-90^\circ$  and thereby, results in a much lower phase margin compared to the CSA model at low frequencies. For the given PI controller, the gain crossover frequencies are almost the same, and the associated phase margins differ by  $5^\circ$ , which is significant relative to the small phase margin available at this low frequency. Figure 15 compares

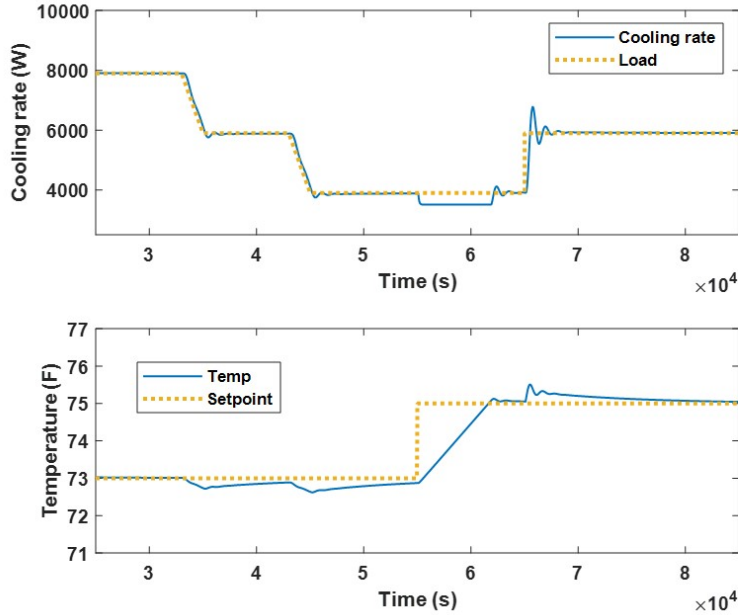


Figure 13: PI+lead control simulation results for case III.

the Bode diagrams and margins of the PI+lead controller for the two load models. Since the lead control action results in an increased gain crossover frequency, the difference in the phase margin between the two load models is reduced to  $2.3^\circ$ . Also, since the absolute margin is significantly higher, the relative margin difference between the two load models is even smaller. This implies that the closed-loop control dynamics will be very similar across the two load models under this fast-responding controller.

To better understand the different closed-loop responses associated with the two load models, a multiplier  $\alpha$  is applied to the PI and PI+lead controllers, i.e.,  $C = \alpha \cdot C_{PI}$  or  $C = \alpha \cdot C_{PI}C_{lead}$ , to achieve different gain crossover frequency and evaluate the margin sensitivity. Figure 16 compares the phase margins for the different control and load model scenarios for  $\alpha$  ranging from

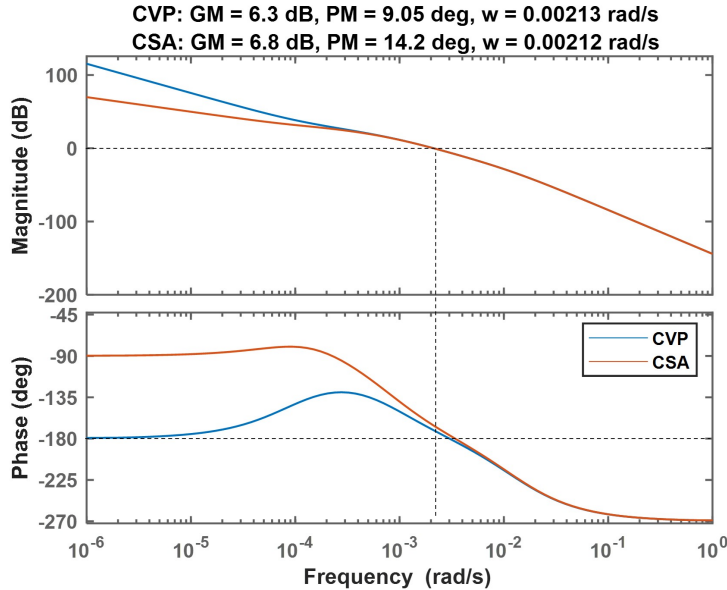


Figure 14: Comparison of PI control Bode diagrams between CSA and CVP load models for case II.

0.1 to 10. It verifies that a faster-responding controller, e.g., the PI+lead controller with a higher gain crossover frequency, is less sensitive to the load model compared to a slower-responding PI controller.

## 7. Experimental Tests of Proposed Controller

The proposed PI+lead controller was implemented in a National Instruments CRIO controller and tested with the same heat pump used for the collection of the native control results presented in Section 2.2. The determined control actions, i.e., the compressor and blower speeds, were sent to the unit's onboard controller through the manufacturer-provided communication protocol. In this remote control mode, the original thermostat was replaced by the proposed controller in the CRIO and thus could not be used for temperature sensing. An emulated thermostat was utilized by feeding the

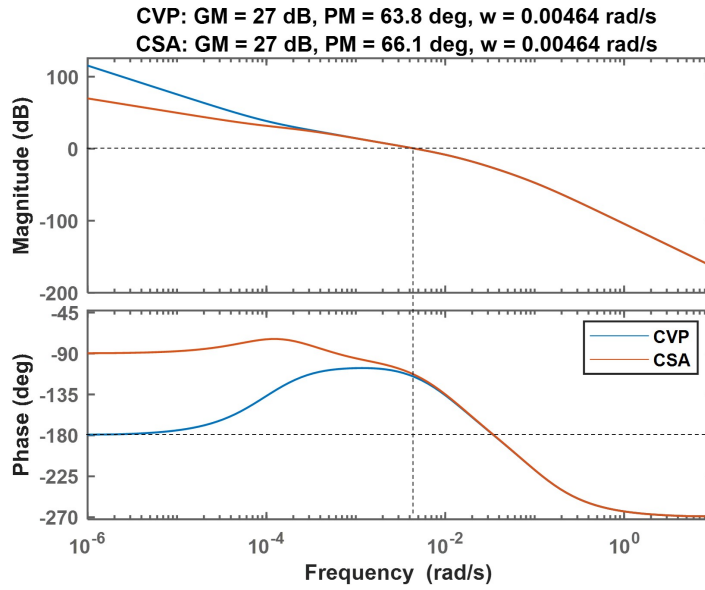


Figure 15: Comparison of PI+lead control Bode diagrams between CSA and CVP load models for case II.

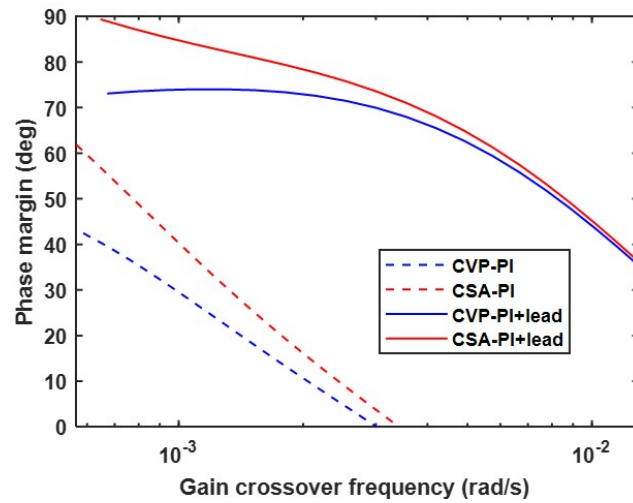


Figure 16: Phase margins of different controllers under CSA and CVP load models for case II.

indoor temperature to the thermostat transfer function shown in Section 3.2, and the emulated thermostat temperature was fed to the PI+lead controller. To verify the impact of chamber dynamics on the closed-loop control performance as discussed in Section 5.3, experimental tests were conducted for two cases, one with the virtual indoor temperature and the other with the return air temperature being fed to the thermostat emulator. The first case resembles Case II by neglecting the chamber dynamics during control decision making, while the latter resembles Case III with chamber dynamics affecting the final control actions. To further demonstrate control performance under fast load-changing conditions, the transitional periods were accelerated from a 1°F/15-minute rate, specified by the CVP, to 1°F/3-minute, resulting in steeper load transitions between intervals that can stress test a heat pump’s load-following performance, with the benefit of reduced test duration. The proposed PI+lead controller was tested with the complete CVP cooling test.

### *7.1. Feedback Control With Virtual Indoor Temperature*

Figure 17 presents the experimental test results for the case with the virtual indoor temperature fed to the thermostat emulator. The controller showed superior load-tracking capability throughout the CVP test, achieving precise load matching throughout all load intervals and transitional periods without overshoot or undershoot. The CVP load profile for the experimental tests was slightly modified, mainly for the low-load interval. According to the CVP, the sensible load during the low-load interval should be set to 103% of the  $F_{low}$  sensible capacity in override mode. However, when communicating with the unit using the manufacturer-provided protocol, the indoor blower speed could not be lowered to the  $F_{low}$  speed. Therefore, the  $F_{low}$  test was

repeated using the minimum speeds allowed in the “remote” control mode and the resultant sensible capacity was chosen as the low load in the CVP test. The compressor and fan speeds were fully synchronized following the same percentage speed setting generated by the controller.

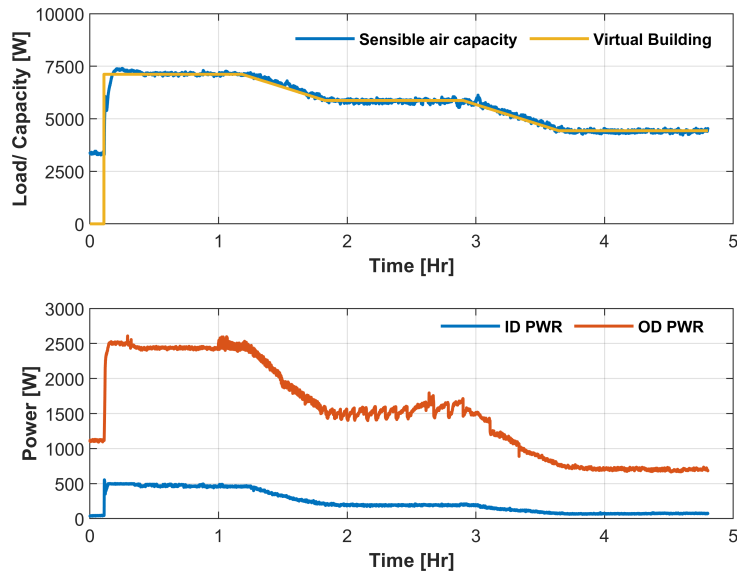


Figure 17: Test unit capacity and power for cooling CVP test under PI+lead controller with virtual indoor temperature input.

Fig. 18 shows the indoor and outdoor temperature variations in the CVP test. Throughout the test, the indoor temperature was well regulated within  $\pm 0.3^{\circ}\text{F}$  around the setpoint. This stable temperature control will provide much improved indoor thermal comfort compared to the native controller that had temperature fluctuations up to  $\pm 2^{\circ}\text{F}$ . The outdoor temperature control achieved by the outdoor chamber’s reconditioning system maintained compliance with the  $1^{\circ}\text{F}$  tolerance specified in the CVP for a majority of the test duration. Occasional drifts outside the tolerance band

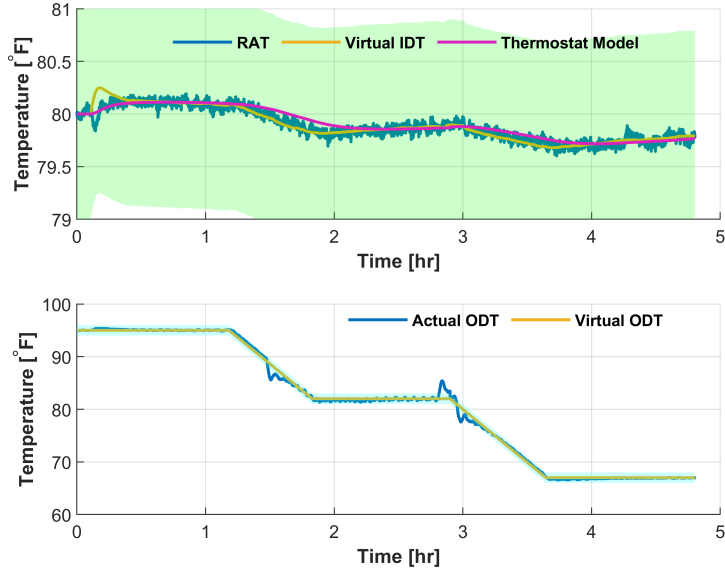


Figure 18: Indoor and outdoor temperature dynamics for cooling CVP test under PI+lead controller with virtual indoor temperature input.

during transitional periods resulted from erratic electric heat control within the psychrometric chamber’s reconditioning system, which employs electric heaters comprised of two heating strips, each providing 50% of the nominal heating capacity. The leading heat strip is modulated continuously with a solid-state relay, while the second strip is only engaged when the heating demand exceeds 50%. Delays in the activation of the secondary heating element produce discontinuous heating capacity transitions when the heating demand crosses 50%, resulting in temperature spikes observed in the outdoor temperature. These outdoor chamber temperature excursions can be easily addressed by retrofitting the chamber heater to enable continuous heat modulation.

## *7.2. Feedback Control With Return Air Temperature*

The CVP test results with the return air temperature (RAT) as input to the thermostat model are displayed in Figures 19 and 20. The test unit cooling capacity followed the virtual building load well throughout the dynamic test, although with more fluctuations compared to the preceding case. The delivered cooling capacity fluctuated within a  $\pm 300$  W band around the load for the duration of the test, caused by the high control temperature fluctuation. Although the thermostat functions as a low-pass filter and helps remove high-frequency noises, the lead action is sensitive to small variations in the control temperature caused by the feedback modulation of the chamber's reconditioning system, resulting in minor control chattering in the closed-loop response. Similar to the previous case, the indoor temperature stayed within  $\pm 0.3^\circ\text{F}$  around the setpoint throughout the test, with a single overshoot outside this bound at the beginning of the CVP test. This high overshoot was caused by the significantly reduced phase margin when chamber dynamics were in play ( $30^\circ$  in Case III versus  $64^\circ$  in Case II). This is also consistent with the simulation results presented in Section 5.3.

Although similar load tracking and temperature control performances were observed (expected as the PI+lead controller was designed to accommodate both Cases II and III), the impact of chamber dynamics on the closed-loop response can be better revealed when the thermostat temperature and control actions of the two cases are compared in Figure 21. In contrast to the smooth sensing temperature in the case with virtual indoor temperature as the thermostat emulator input, using the RAT for thermostat control resulted in small oscillations in the sensing temperature and, in turn,

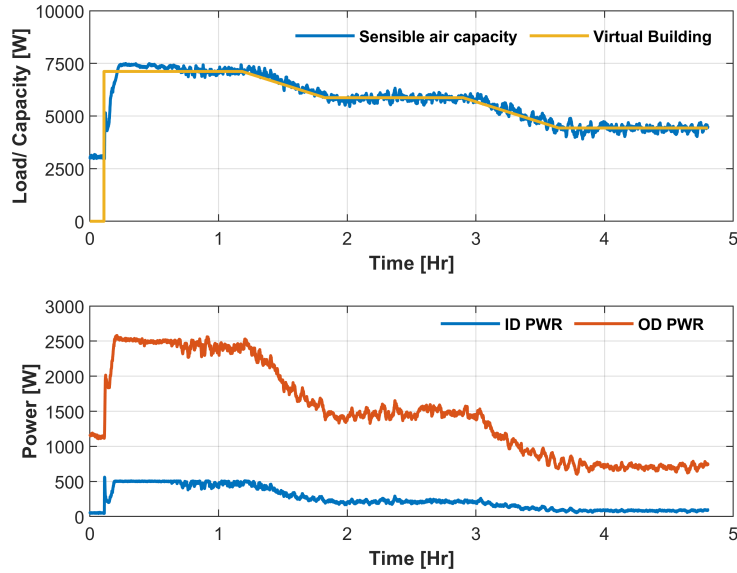


Figure 19: Test unit capacity and power for cooling CVP test under PI+lead controller with RAT input.

the control action. In addition, the chamber dynamics led to some minor delays in the sensing temperature and control actions.

The resultant oscillatory control actions for the compressor and fan speeds disturbed the superheat control. Figure 22 compares the electronic expansion valve (EXV) and superheat control behaviors between the two cases. The EXV PI controller, designed in a previous study [34], showed satisfactory superheat control performance for the case with the virtual indoor temperature as the thermostat emulator input. However, for the test with the RAT used as the thermostat input, the superheat fluctuated significantly due to the disturbance from the oscillatory compressor and fan speeds.

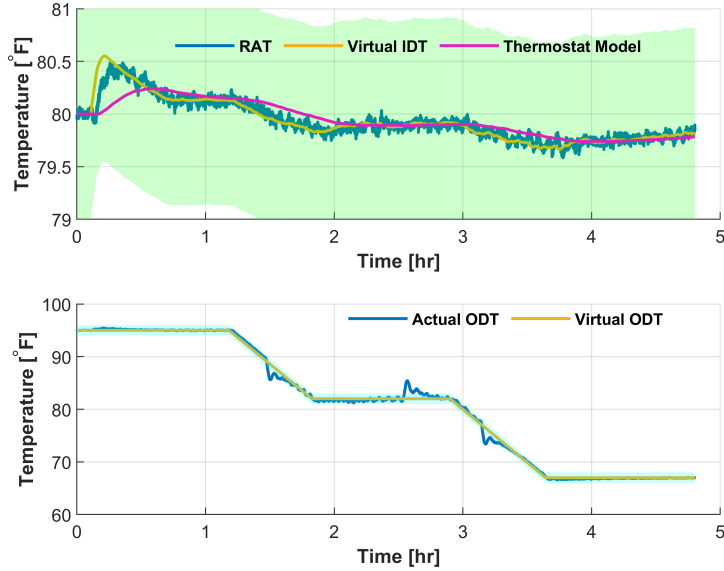


Figure 20: Indoor and outdoor temperature dynamics for cooling CVP test under PI+lead controller with RAT input.

### 7.3. CSA Load Model Test With Feedback Control Using Virtual Indoor Temperature

To verify the performance of the PI+lead controller under the CSA load model discussed in Section 6, experimental tests were repeated following the three load intervals in the CVP, but using the CSA equation to update the virtual indoor temperature. To ensure fair comparisons, modifications were made to the outdoor temperature profile to achieve consistent load ratios across the three load intervals between the CVP and CSA tests. The design outdoor balance point of  $67^{\circ}\text{F}$  was used for this test, and the balance point was updated according to the instantaneous indoor temperature per the CSA load model. The test was conducted using the virtual indoor temperature as the thermostat emulator input.

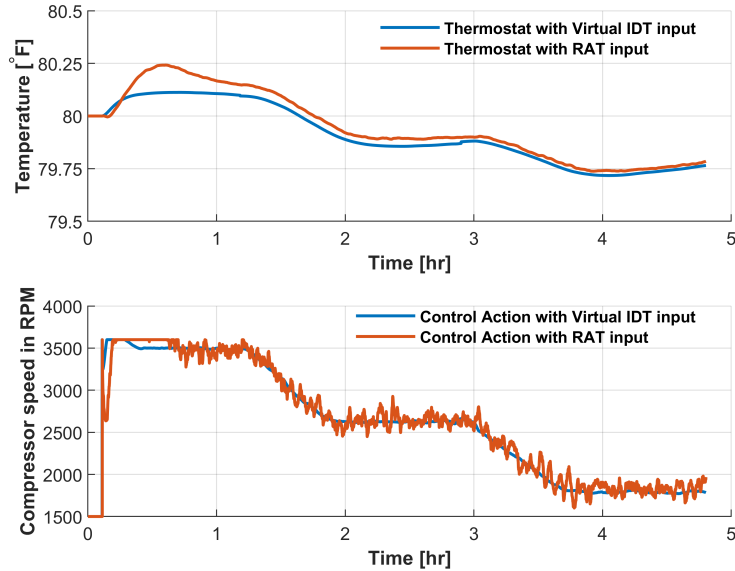


Figure 21: Impact of chamber dynamics on thermostat temperature and PI+lead controller under the CVP test.

Figures 23 and 24 display the control performance of the PI+lead controller under the CSA load model. The controller exhibited very similar behaviors to those seen in the CVP tests. The outdoor temperature traversed a smaller range (94°F to 83°F) for this test because of the steeper load line with the outdoor temperature. Temperature excursions were still observed in the outdoor chamber caused by the improper control of the electric heater in the psychrometric chamber's reconditioning system. These results validate the load model impact analysis presented in Section 6 that the virtual load model has a negligible impact on the closed-loop response for a fast-responding controller.

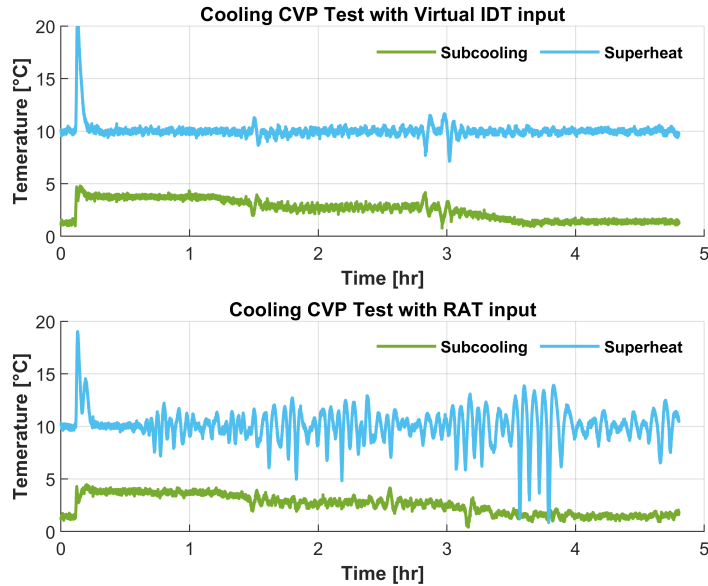


Figure 22: Impact of chamber dynamics on superheat control performance.

## 8. Discussion

The experimental test results agree well with the CVP and CSA simulation test results presented in Sections 5 and 6, which validates the control analyses presented therein. The improved control performance achieved with the proposed controller can bring a variety of benefits including but not limited to:

- Pass the CVP and earn a variable-speed certification (current test results can only certify the unit with the native controller as a two-stage unit, with lower SEER and HSPF ratings).
- Increase the heat pump life expectancy with reduced control actuation of the compressor and fans.

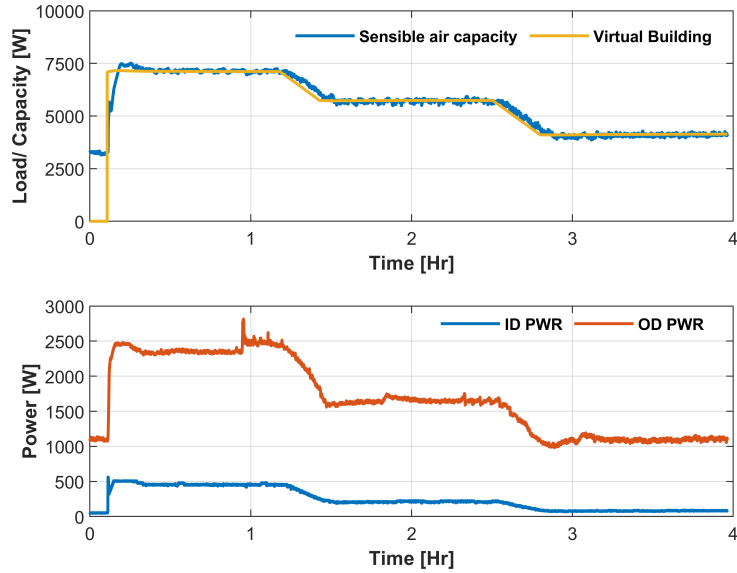


Figure 23: Test unit capacity and power for cooling CSA test under PI+lead controller with virtual indoor temperature input.

- Improve indoor comfort with more stable indoor temperature control.
- Reduce test burden for manufacturers/third-party assessors.

The control analysis and experimental tests highlight the following issues and questions that need to be addressed with the current load-based testing methodology:

- Chamber dynamics can lead to mischaracterization of a heat pump's field performance in a load-based test. A Thermostat Environment Emulator (TEE) [33] or improved chamber control strategies, e.g., model predictive control, should be used to achieve fast control of the thermostat environment.

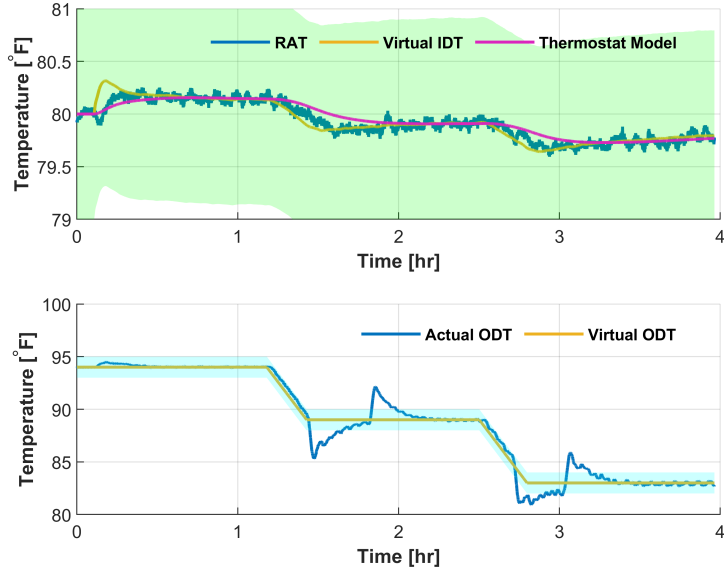


Figure 24: Indoor and outdoor temperature dynamics for cooling CSA test under PI+lead controller with virtual indoor temperature input.

- Thermostat dynamics and their locations can affect the overall control performance. CSA SPE-07 allows the placement of the thermostat in the return air stream, which can result in much faster temperature response compared to a field installation. Using TEE could help remove thermostat location dependence and achieve improved repeatability and reproducibility of load-based tests.
- Different virtual load models, e.g., those adopted by CVP and CSA, can lead to different closed-loop responses for a slow-responding controller; however, the impact is negligible for fast-responding controllers.
- Traditional PI controllers are not able to provide satisfactory control performance, mainly caused by the slow thermostat dynamics. Lead

control actions (even cascaded lead controllers) are needed to achieve fast and stable closed-loop responses.

## 9. Conclusions

Motivated by the control issues observed in previous load-based tests conducted on different residential and commercial ACHP systems, a framework for control stability and performance analysis was developed based on a linear dynamic simulation toolkit and utilized for control analysis of load-based testing under different thermostat and testing chamber dynamics. Results show that slow thermostat and chamber dynamics can cause control challenges using traditional PI controllers - a fast-responding PI controller may be unstable, while a stable PI controller has a response too slow for proper operation of a heat pump in the field. A PI plus lead controller was proposed to boost the phase and achieve fast yet stable control with adequate stability margins. The control analysis also showed that the inclusion of the testing facility's dynamics could prompt oscillatory or even unstable control behaviors, which may not represent a heat pump's field performance. The CSA load-based testing procedure and the CVP involve two different types of virtual load models. To assess the impact of the virtual load model form on the load-based testing performance, control analyses were conducted with the CSA and CVP load models, and the results show negligible differences for fast-responding controllers. However, for slow-responding controllers, the CSA virtual load model would result in greater phase margins. All the analyses were validated with experimental tests using a 3-ton variable-speed heat pump.

This study focused on control performance analyses for the load-based testing procedures specified in CSA SPE-07 and AHRI 210/240 Appendix I. There exist substantial differences between the two testing procedures, e.g., regarding the placement of thermostats and the virtual load model adopted, that can lead to quite different rating outcomes. Further investigations should expand the analysis to cover load-based testing procedures specified in other regional standards and different types of testing facilities, e.g., the closed-loop test apparatus proposed in [35]. This will generate more insights into the robustness of the developed PI plus lead controller and potential improvements of these standards to incentivize ACHP manufacturers to innovate and deliver more efficient products with certified field performance.

## References

- [1] Jie Ma, Chibuoke Eneh, Dongyang Xi, James E. Braun, W. Travis Horton, and Jie Cai. Control performance analysis of load-based testing for air-conditioning and heat pump systems: Part i - control oriented simulation model development. *Energy and Buildings*, 2025. submitted.
- [2] AHRI Standard 210/240: Performance rating of unitary air-conditioning and air-source heat pump equipment, 2023.
- [3] Steve P Kavanaugh. Limitations of SEER for measuring efficiency. *ASHRAE journal*, 44(7):27–28, 2002.
- [4] Lars Nolting, Simone Steiger, and Aaron Praktijnjo. Assessing the

- validity of European labels for energy efficiency of heat pumps. *Journal of Building Engineering*, 18:476–486, 2018.
- [5] SPE-07:23: Draft experimental standard for load-based testing of residential air conditioners and heat pumps. Technical report, CSA Group, 2024. CSA Group, Toronto, ON, Canada. Draft standard.
- [6] Lorenzo Cremaschi and Pedro Perez Paez. Experimental feasibility study of a new load-based method of testing for light commercial unitary heating, ventilation, and air conditioning (ASHRAE RP-1608). *Science and Technology for the Built Environment*, 23(7):1178–1188, 2017.
- [7] Andrew L Hjortland and James E Braun. Load-based testing methodology for fixed-speed and variable-speed unitary air conditioning equipment. *Science and Technology for the Built Environment*, 25(2):233–244, 2019.
- [8] Akash Patil, Andrew L Hjortland, Li Cheng, Parveen Dhillon, James E Braun, and W Travis Horton. Load-based testing to characterize the performance of variable-speed equipment. *International Refrigeration and Air Conditioning Conference*, 2018.
- [9] Li Cheng, Parveen Dhillon, W Travis Horton, and James E Braun. Automated laboratory load-based testing and performance rating of residential cooling equipment. *International Journal of Refrigeration*, 123:124–137, 2021.
- [10] Parveen Dhillon, Akash Patil, Li Cheng, James E Braun, and W Travis Horton. Performance evaluation of heat pump systems based on a load-

- based testing methodology. *International Refrigeration and Air Conditioning Conference*, 2018. Paper 2077.
- [11] Parveen Dhillon, W Travis Horton, and James E Braun. Comparison of steady-state and dynamic load-based performance evaluation methodologies for a residential air conditioner. *International Refrigeration and Air Conditioning Conference*, 2021. Paper 2172.
- [12] Parveen Dhillon, Drew Welch, Brian Butler, W Travis Horton, and James E Braun. Validation of a load-based testing method for characterizing residential air-conditioner performance. *International Refrigeration and Air Conditioning Conference*, 2021. Paper 2257.
- [13] Parveen Dhillon, Li Cheng, W Travis Horton, and James E Braun. Laboratory load-based testing and performance rating of residential heat pumps in heating mode. *Science and Technology for the Built Environment*, 29(1):49–64, 2023.
- [14] Rolf Isermann, Jochen Schaffnit, and Stefan Sinsel. Hardware-in-the-loop simulation for the design and testing of engine-control systems. *Control Engineering Practice*, 7(5):643–653, 1999.
- [15] Bin Lu, Xin Wu, Hernan Figueroa, and Antonello Monti. A low-cost real-time hardware-in-the-loop testing approach of power electronics controls. *IEEE Transactions on Industrial Electronics*, 54(2):919–931, 2007.
- [16] Jonathan Millitzer, Dirk Mayer, Christian Henke, Torben Jersch, Christoph Tamm, Jan Michael, and Christopher Ranisch. Recent de-

- velopments in hardware-in-the-loop testing. In *Model Validation and Uncertainty Quantification, Volume 3: Proceedings of the 36th IMAC, A Conference and Exposition on Structural Dynamics 2018*, pages 65–73. Springer, 2018.
- [17] J. Lebrun and S. Wang. BEMS: Evaluation and emulation techniques — synthesis report. Technical report, International Energy Agency (IEA) ECBCS Annex 17; University of Liège, Laboratory of Thermodynamics, Liège, Belgium, March 1993. IEA ECBCS Annex 17.
- [18] R Lahrech, P Gruber, P Riederer, P Tessier, and JC Visier. Development of a testing method for control HVAC systems by emulation. *Energy and buildings*, 34(9):909–916, 2002.
- [19] Philipp Mehrfeld, Markus Nürenberg, Martin Knorr, Lars Schinke, Maximilian Beyer, Manuel Grimm, Moritz Lauster, Dirk Müller, Joachim Seifert, and Konstantinos Stergiaropoulos. Dynamic evaluations of heat pump and micro combined heat and power systems using the hardware-in-the-loop approach. *Journal of Building Engineering*, 28:101032, 2020.
- [20] Lilli Frison, Martin Kleinstück, and Peter Engelmann. Model-predictive control for testing energy flexible heat pump operation within a hardware-in-the-loop setting. In *Journal of Physics: Conference Series*, volume 1343, page 012068. IOP Publishing, 2019.
- [21] Wessam El-Baz, Lukas Mayerhofer, Peter Tzscheutschler, and Ulrich Wagner. Hardware in the loop real-time simulation for heating systems: Model validation and dynamics analysis. *Energies*, 11(11):3159, 2018.

- [22] Zhimin Jiang, Jie Cai, and Paul S Moses. Smoothing control of solar photovoltaic generation using building thermal loads. *Applied Energy*, 277:115523, 2020.
- [23] Reid Hart, Dan Morehouse, Will Price, John Taylor, Howard Reichmuth, and Mark Cherniack. Up on the roof: From the past to the future. *ACEEE Summer Study on Energy Efficiency in Buildings*, 2008.
- [24] Qi Qi and Shiming Deng. Multivariable control of indoor air temperature and humidity in a direct expansion (DX) air conditioning (A/C) system. *Building and Environment*, 44(8):1659–1667, 2009.
- [25] Huaxia Yan, Yudong Xia, Xiangguo Xu, and Shiming Deng. Inherent operational characteristics aided fuzzy logic controller for a variable speed direct expansion air conditioning system for simultaneous indoor air temperature and humidity control. *Energy and Buildings*, 158:558–568, 2018.
- [26] Jie Cai and James E Braun. A generalized control heuristic and simplified model predictive control strategy for direct-expansion air-conditioning systems. *Science and Technology for the Built Environment*, 21(6):773–788, 2015.
- [27] Niccolo Giannetti, Shun Matsui, Ryohei Mori, Jongsoo Jeong, Hifni Mukhtar Ariyadi, Yoichi Miyaoka, Eisuke Togashi, and Kiyoshi Saito. Emulator-type load-based tests for dynamic performance characterization of air conditioners. *Energy and Buildings*, 273:112411, 2022.

- [28] Niccolo Giannetti, A Mizuno, Y Miyaoka, Y Sei, K Enoki, K Saito, et al. Feed-forward compensation for emulator-type testing facilities. *International Journal of Refrigeration*, 167:257–268, 2024.
- [29] Jie Ma, Parveen Dhillon, W Travis Horton, and James E Braun. Heat-pump control design performance evaluation using load-based testing. *International Refrigeration and Air Conditioning Conference*, 2021. Paper 2173.
- [30] S Kia Mossalaei, Jie Ma, Parveen Dhillon, Jie Cai, W. Travis Horton, and James Braun. Laboratory evaluation of control verification procedures for certification of variable-speed heat pumps. *ASHRAE Annual Conference*, 2025.
- [31] MathWorks, Inc. *ocr: Optical Character Recognition*, 2024. Computer Vision Toolbox, MATLAB R2024a.
- [32] Jin Wen and Theodore F Smith. Effect of thermostat time constant on temperature control and energy consumption. In *SIcon/01. Sensors for Industry Conference. Proceedings of the First ISA/IEEE. Sensors for Industry Conference (Cat. No. 01EX459)*, pages 252–257. IEEE, 2001.
- [33] Li Cheng, James E Braun, and W Travis Horton. Load-based testing using a thermostat environment emulator. *International Journal of Refrigeration*, 126:109–122, 2021.
- [34] Haopeng Liu, Jie Cai, and Donghun Kim. A hierarchical gray-box dynamic modeling methodology for direct-expansion cooling systems to

support control stability analysis. *International Journal of Refrigeration*, 133:191–200, 2022.

- [35] Dohyeon Kim, Parveen Dhillon, Ashwin Kidambi, Travis Horton, and James E Braun. Closed-loop apparatus (CLA) design and assessment for load-based testing. *International Refrigeration and Air Conditioning Conference*, 2024. Paper 2679.